



3D-Printed PCL/Zn scaffolds for bone regeneration with a dose-dependent effect on osteogenesis and osteoclastogenesis



Siyi Wang^{a,b}, Ranli Gu^{a,b}, Feilong Wang^{a,b}, Xiao Zhao^{a,b}, Fan Yang^{a,b}, Yuqian Xu^{a,b},
Fanyu Yan^{a,b}, Yuan Zhu^{a,b}, Dandan Xia^{b,c,**}, Yunsong Liu^{a,b,*}

^a Department of Prosthodontics, Peking University School and Hospital of Stomatology, Beijing, 100081, China

^b National Center of Stomatology, National Clinical Research Center for Oral Diseases, National Engineering Laboratory for Digital and Material Technology of Stomatology, Beijing Key Laboratory of Digital Stomatology, Research Center of Engineering and Technology for Computerized Dentistry Ministry of Health, NMPA Key Laboratory for Dental Materials, No.22, Zhongguancun South Avenue, Haidian District, Beijing, 100081, PR China

^c Department of Dental Materials, Peking University School and Hospital of Stomatology, Beijing, 100081, China

ARTICLE INFO

Keywords:

Polycaprolactone
Zinc
Osteogenesis
Osteoclastogenesis
3D-printed scaffolds

ABSTRACT

Polycaprolactone (PCL) is a polymer material suitable for being prepared into porous scaffolds used in bone tissue engineering, however, insufficient osteogenic ability and mechanical strength limit its application. Zinc (Zn) alloy with proper mechanical strength and osteogenesis is a promising biodegradable metal that have attracted much attention. Herein, we combined the advantages of PCL and Zn by fabricating PCL/Zn composite scaffolds with different Zn powder contents (1 wt%, 2 wt%, 3 wt%) through fused deposition modelling. The mechanical property, cytocompatibility and Zn ions release behavior of PCL/Zn scaffolds were analyzed *in vitro*. The osteogenesis and osteoclastogenesis properties of the scaffolds were evaluated by being implanted into Sprague–Dawley rats calvaria defect. Results showed that the PCL/Zn scaffolds exhibited improved mechanical properties and cytocompatibility compared with the pure PCL scaffolds. At 8 weeks after *in vivo* implantaion, the addition of Zn powder promoted new bone formation, in a dose-dependent manner. The scaffolds with 2 wt% Zn displayed the best osteogenic effect, while the osteogenic effect was slightly reduced in the scaffolds with 3 wt% Zn. In the studied Zn contents, the PCL/Zn scaffolds gradually promoted osteoclastogenesis with increased Zn content. In the 3 wt% Zn group, TRAP-positive cells were observed on the newly formed bone edges around the scaffolds. These dose-dependent effects were verified *in vitro* using MC3T3-E1 and RAW264.7 cells. Finally, we revealed that Zn²⁺ regulated osteogenesis and osteoclastogenesis by activation of the Wnt/ β -catenin and NF- κ B signalling pathways, respectively.

1. Introduction

Although bone tissue has the ability to repair and regenerate itself, a large volume of bone loss caused by tumour resection, injuries, infection or severe trauma may exceed the self-repair ability [1–3]. For bone defect treatment, autologous bone transplantation has always been the “gold standard”, however, it has limitations such as high incidence of defects and infection at the donor sites [4–6]. Therefore, there is an urgent need to develop new bone substitutes to meet the clinical needs. Bone tissue engineering (BTE), which has emerged in recent decades, now provides

an option for the treatment of bone defects [8,9]. Porous scaffolds have the advantages of adjustable mechanical strength and sufficient cell ingrowth permeability, and are expected to be the most favourable candidate materials for bone substitutes [12].

Three-dimensional (3D) printing technology accelerated the development of BTE, since it provides the possibility of producing custom scaffolds with 3D geometry, internal structure and architecture [10,11]. 3D printing is a set of production processes defined as “a process of joining materials to create objects from 3D model data, usually layer-by-layer” by American Society of Testing Materials (ASTM) [13]. A

* Corresponding author. Department of Prosthodontics, Peking University School and Hospital of Stomatology, No.22, Zhongguancun South Avenue, Haidian District, Beijing, 100081, China.

** Corresponding author. Department of Dental Materials, Peking University School and Hospital of Stomatology, No.22, Zhongguancun South Avenue, Haidian District, Beijing, 100081, China.

E-mail addresses: dandanxia@pku.edu.cn (D. Xia), liuyunsong@hsc.pku.edu.cn (Y. Liu).

<https://doi.org/10.1016/j.mtbio.2021.100202>

Received 24 October 2021; Received in revised form 20 December 2021; Accepted 29 December 2021

Available online 1 January 2022

2590-0064/© 2022 The Authors. Published by Elsevier Ltd. This is an open access article under the CC BY-NC-ND license (<http://creativecommons.org/licenses/by-nc-nd/4.0/>).

variety of polymers commonly applied in 3D printing have been used in bone regeneration, including polycaprolactone (PCL) and its copolymers. Among which PCL show great advantage in 3D printing bone scaffolds. Approved by the United States Food and Drug Administration (FDA), PCL has been widely used due to its good biocompatibility and ease of processing (melting point: 55–60°C). In addition, the composition and structure of PCL are adjustable [14,15]. However, when used alone, PCL and its degradation products do not exhibit osteogenic properties [16]. Moreover, when pure PCL is used as a tissue engineering scaffold, its mechanical properties are usually unsatisfactory [17].

Zinc (Zn) and its alloys are becoming promising biomaterials due to their favourable mechanical strength, degradation rates and biocompatibility. Moreover, their degradation products are completely bioresorbable without generating hydrogen gas [19–21]. In addition, Zn is an essential trace element for the human body and participates in basic life processes, such as energy metabolism and protein synthesis [22,23]. In the human body, 85% of Zn is located in muscle and bone. Moreover, Zn has a stimulating effect on bone formation and mineralisation. Meanwhile, Zn deficiency can delay bone metabolism and retard bone growth [24]. Therefore, incorporating Zn into the pure PCL scaffold provides a feasible method to improve the osteogenesis and mechanical properties of PCL.

Studies have shown that, during bone formation, Zn^{2+} promotes osteoblast proliferation and differentiation, as well as collagen synthesis [25,26]. The effect of Zn^{2+} on osteogenic processes shows a biphasic dose response. Previous research noted that the positive effect of Zn^{2+} on osteoblast activity occurs within a narrow dose range (1–50 μM); doses exceeding 50 μM inhibit osteogenic activity, while below 1 μM there is no measurable effect [27]. However, reports on the role of Zn^{2+} in osteoclastogenesis are inconsistent [28,29]. Some reports indicate that sub-nanomolar Zn^{2+} can inhibit osteoclastogenesis [30]. On the contrary, Holloway et al. reported that a Zn^{2+} concentration of 10^{-4} mol/L increased the number of tartrate-resistant acid phosphatase (TRAP)-positive cells when co-cultured with osteoblast-like cells [31]. Thus, it is worthy to further explore the role of Zn^{2+} on osteoclastogenesis for better bone regeneration.

In this study, PCL/Zn composite scaffolds with different Zn powder contents (1 wt%, 2 wt%, 3 wt%) were fabricated through fused deposition modelling (FDM). Then, the mechanical property, cytocompatibility and Zn ions release behavior of PCL/Zn scaffolds were analyzed *in vitro*. The osteogenesis and osteoclastogenesis properties of the composite scaffolds were evaluated in rats calvaria defect. Besides, MC3T3-E1 cells and RAW264.7 cells were used to assess the effect of different Zn^{2+} concentrations on osteogenesis and osteoclastogenesis *in vitro*. Finally, the underlying mechanisms for osteogenesis and osteoclastogenesis were explored.

2. Materials and methods

2.1. PCL/Zn scaffold preparation and characterisation

PCL (Mn = 37,000 Da) pellets were obtained from Shinuo Technology Co., Ltd (Beijing, China) and pure Zn powder (diameter = 2–5 μm , 99.99% in purity) were obtained from Yufeng Zheng's lab (Peking University, Beijing, China). PCL/Zn composite particles were prepared by melt compounding method. PCL pellets were heated to 120 °C to melt and Zn powder were added and mixed at the ratio of 1, 2, 3 wt% to form PCL/Zn blends. Then the material was drawn into filaments and cut into clumps no more than 1 cm in length to feed into the 3D printer inlet. Following the fused deposition modelling (FDM), Geomagic Studio 2012 software (Raindrop Geomagic, Rock Hill, SC, USA) was used for computer-aided design (CAD) and the Elements Mixture-I bioprinter (Shinuo Technology Co., Ltd., China) was used for manufacturing the scaffolds. The nozzle size was 300 μm and feed rate was 500 mm/min. The filament distance (FD) and layer thickness of the fabricated scaffolds were both 300 μm (pore size of 300 μm and porosity of 50%), and the lay-

down pattern was 0/90°. The scaffolds were divided into four groups: pure PCL (PCL), PCL with 1 wt% Zn (PCL-1Zn), PCL with 2 wt% Zn (PCL-2Zn) and PCL with 3 wt% Zn (PCL-3Zn).

2.1.1. Immersion testing

For Zn ions release behavior, samples were immersed in simulated body fluid at 37°C. The ratio of sample weight to solution volume was 0.1 g/ml. The concentration of Zn^{2+} in the extracts was measured on days 1, 3, 5, 7, 9, 11, 13 and 15 by inductively coupled plasma emission spectrometry (ICP-OES; iCAP6300; Thermo Fisher Scientific, Waltham, MA, USA).

2.1.2. Morphological characterisation

The structure and surface morphology of the scaffolds were inspected by scanning electron microscopy (SEM; EVO 18; Zeiss, Oberkochen, Germany) at an accelerating voltage of 10 kV. The actual strut diameter, pore size and layer thickness were measured through the obtained scaffold surface and cross-sectional images. Elemental analysis was performed using an energy-dispersive spectrometer (EDS; INCA X-Act; Oxford Instruments, Abingdon, UK) attached to the SEM.

The Archimedes principle was used to measure the porosity of the scaffold. Ethanol (density ρ_e) was used as the replacement fluid. A density bottle filled with ethanol was weighed (W_1). A scaffold sample weighing W_S was immersed into the density bottle, and the air bubbles in the scaffold pores were evacuated. Then ethanol was added to the density bottle to full and weighed (W_2). The scaffold saturated with ethanol was removed from the density bottle and then the density bottle was weighed (W_3). The volume of the scaffold pore (V_p) and the volume of the scaffold skeleton (V_s) was calculated to obtain the porosity value (ϵ). The following formulas were used to carry out the calculations.

$$V_p = (W_2 - W_3 - W_S) / \rho_e$$

$$V_s = (W_1 - W_2 + W_S) / \rho_e$$

$$\epsilon = V_p / (V_p + V_s) = (W_2 - W_3 - W_S) / (W_1 - W_3).$$

2.1.3. Mechanical properties

The mechanical properties were measured under compression and three-point flexure according to the ASTM standard D695-02a. In the compression test, each group contained five cylindrical samples (5 mm diameter \times 10 mm height) and the loading rate was 5 mm/min. In the three-point flexure test, samples of dimensions 10 \times 30 mm² were prepared; the constant loading rate was 1 mm/min. An electronic universal testing machine (Z020; ZwickRoell, Ulm, Germany) was used to obtain the stress–strain curve. The elastic modulus was calculated from the initial linear part of the curve.

2.1.4. Contact angle measurement

Solid samples were prepared to conduct this measurement. Briefly, the melted PCL/Zn filaments of different groups were extruded onto the 3D printer platform, and the materials were pressed into a thickness of about 300 μm by a smooth glass plate. In order to eliminate the influence of the surface roughness of the samples, we selected the area on the surface as smooth as possible, measured the surface roughness (Ra value) using a profilometer (SJ-400, Mitutoyo, Japan), and then carried out the contact angle experiment. A contact angle system (KINO Scientific Instrument, Boston, MA, USA) was used to measure surface hydrophilicity. Briefly, a water drop (1 μl) was added to the sample surface and the contact angle was measured after 30 s.

2.1.5. Cell cytotoxicity of scaffolds

Live/dead staining test was conducted to evaluate the *in vitro* cytotoxicity of the scaffolds. The scaffolds were placed in 24-well plates and 500 μl MC3T3-E1 cell suspension was seeded on each scaffold at a density

of 1×10^6 cells/ml. After incubation for 12 h, the scaffolds were immersed in phosphate-buffered saline (PBS) containing 4 mM of calcein acetoxymethyl ester (calcein AM) and 16 mM of propidium iodide (PI) for 30 min. Dead cells (PI, red) and calcein live cells (AM, green) were observed under a confocal microscope (Axiovert 650; Carl Zeiss Micro-Imaging, Oberkochen, Germany) at excitation wavelengths of 543 and 488 nm, respectively.

2.2. *In situ* osteogenesis and osteoclastogenesis of scaffolds *in vivo*

Our research was approved by the Ethics Committee of Peking University Health Science Center (LA 2019019). Animal experiments were carried out in accordance with the protocol formulated by the Laboratory Animal Ethics Branch. To minimise potential suffering, all animals were anaesthetised with sodium pentobarbital (50 mg/kg). Thirty 8-week-old Sprague–Dawley (SD) rats were randomly divided into the five groups ($n = 6$): PCL, PCL-1Zn, PCL-2Zn, PCL-3Zn and blank control. On the right side of the calvaria of each rat, a full-thickness defect with a diameter of 6 mm was prepared with a trephine. In the experimental groups, scaffolds with a diameter of 6 mm and thickness of 1.5 mm were implanted in the defects, while in the blank control group, the defects were left empty.

Eight weeks post-surgery, rats were sacrificed under anaesthesia and the calvaria with implanted scaffolds were harvested. To assess the differences in bone mass and microstructure, a high-resolution Inveon device (Siemens, Munich, Germany) was used to perform X-ray micro-computed tomography (micro-CT) scans. Three-dimensional visualisation software (Inveon Research Workplace; Siemens) was used for 3D reconstruction of images. The microstructure parameters of bone mineral density (BMD) and bone volume (BV) were then calculated. After micro-CT analysis, the remaining calvaria specimens were decalcified, embedded, sectioned and histologically examined by H&E, Masson, TRAP and OCN immunohistochemical staining. Subsequently, TRAP-positive cells per mm^2 were counted.

2.3. *In vitro* osteogenic properties of Zn^{2+}

Mouse osteoblast-like cells (MC3T3-E1) were used for *in vitro* osteogenic experiments. The proliferation medium (PM) consisted of Dulbecco's modified Eagle's medium (DMEM) containing 10% foetal bovine serum, 100 U/m penicillin and 100 $\mu\text{g}/\text{mg}$ streptomycin. Then, 10 mM β -glycerophosphate, 10 nM dexamethasone and 50 $\mu\text{g}/\text{ml}$ L-ascorbic acid were added to the PM to form an osteogenic medium (OM), which was used for osteogenic induction. Zinc sulphate was separately added to the PM and OM to prepare aqueous solutions with Zn^{2+} concentrations of 1, 2, 3 and 4 mg/L. The cells were cultured at 37°C in a humidified atmosphere of 5% CO_2 .

2.3.1. Cell proliferation assay

To study the effect of Zn^{2+} on the proliferation and viability of MC3T3-E1 cells, cells were seeded in 24-well plates at a density of 1×10^4 cells per well. Then cell counting kit 8 (CCK-8; Dojindo Laboratories, Kumamoto, Japan) assay was conducted after 1, 3, 5 and 7 days of culture. A microplate reader was used to measure the optical density (OD; absorbance) value at 450 nm.

2.3.2. Alkaline phosphatase (ALP) activity

Cells were seeded in 12-well plates at a density of 2×10^4 cells per well for ALP activity assays. Seven days after osteogenic induction, ALP staining was performed using the nitro blue tetrazolium (NBT)/5-bromo-4-chloro-3-indolyl phosphate (BCIP) staining kit (CoWin Biotech, Beijing, China). At the same time point, the ALP assay kit (Beyotime, Shanghai, China) was used to quantify ALP activity. Absorbance at 520 nm was measured and the ALP activity was calculated.

Table 1

Primer pairs used in quantitative real-time PCR.

Gene	Forward primer	Reverse primer
Gapdh	5'-ACCACAGTCCATGCCATCAC-3'	5'-TCCACCACCTGTTGCTGTA-3'
Alp	5'-GAGCGTCATCCCAGTGGAG-3'	5'-TAGCGGTTACTGTAGACACCC-3'
Runx-2	5'-TTCAACGATCTGAGATTTGTGGG-3'	5'-GGATGAGGAATGCGCCCTA-3'
Trap	5'-CAGCAGCCAAGGAGGACTAC-3'	5'-ACATAGCCACACCGTTCTC-3'
c-Fos	5'-ATGGGCTCTCCTGTCAACAC-3'	5'-GGCTGCCAAAATAAACTCCA-3'
Axin2	5'-TGACTCTCCTCCAGATCCA-3'	5'-TGCCCACTAGGCTGACA-3'
Lrp5	5'-CTGCCAGGATCGCTCTGATG-3'	5'-ACACTGTTGCTGTATGAGGACACAC-3'
RANKL	5'-AGCCGAGACTACGGCAAGTA-3'	5'-GCGCTCGAAAGTACAGGAAC-3'
RANK	5'-GCTGGTACCCTGGAAC-3'	5'-GTGCACTGGTCCAAGTTT-3'

2.3.3. Alizarin Red S (ARS) staining and quantification of mineralisation

Cells were also seeded in 12-well plates at a density of 2×10^4 cells per well. Fourteen days after osteogenic induction, the samples were stained with 2% Alizarin Red buffer (Sigma–Aldrich, St. Louis, MO, USA). To quantify mineral accumulation, a 100 mM cetylpyridine solution was added to release any calcium-bound ARS into the solution. After complete dissolution, the OD value at 562 nm was measured.

2.3.4. Quantitative real-time PCR (RT-PCR)

Cells were seeded in 6-well plates at a density of 5×10^4 cells per well. TRIzol reagent (Invitrogen, Carlsbad, CA, USA) was used to extract total cellular RNA from cells cultured for 7 days. RT-PCR was performed using the ABI Prism 7500 RT-PCR system (Applied Biosystems, Foster City, CA, USA) with SYBR Green Master Mix. *Gapdh* was used as a reference gene. The primer sequences of mouse *Gapdh*, *Alp* and *Runx2* are listed in Table 1.

2.4. *In vitro* osteoclastic properties of Zn^{2+}

RAW 264.7 cells, a cell line derived from murine macrophages, were used for *in vitro* osteoclastogenesis experiments. PM was prepared as described above, and recombinant mouse receptor activator of nuclear factor-kappa B ligand (RANKL, 50 ng/ml) and recombinant mouse macrophage colony stimulating factor (M-CSF, 50 ng/ml) were then added to PM to constitute osteoclast conditioned medium (OCM). Zinc sulphate was separately added to the PM and OCM to prepare aqueous solutions with Zn^{2+} concentrations of 1, 2, 3 and 4 mg/L.

2.4.1. Cell proliferation assay

To study cell proliferation and viability, RAW264.7 cells were seeded in 24-well plates at a density of 1×10^4 cells per well, cells were exposed to PM containing Zn^{2+} for 1, 3, 5 and 7 days, and the CCK-8 assay was conducted as described above.

2.4.2. TRAP activity assay

Cells were seeded in 12-well plates at a density of 2×10^4 cells per well. Seven days after OCM culture, TRAP staining was performed using the TRAP kit (Sigma–Aldrich) to evaluate the formation of osteoclasts. TRAP-positive cells with more than three nuclei were considered osteoclasts. For quantitative analysis of TRAP activity, cells were lysed; an acid phosphatase detection kit (Beyotime) was used and the OD at 405 nm was measured.

2.4.3. Quantitative RT-PCR

Cells were seeded in 6-well plates at a density of 5×10^4 cells per well. Total cellular RNA was extracted from cells cultured in PM and OCM for 7 days. Subsequent experiments were carried out as described

above in 2.3.4. The primer sequences of mouse *Gapdh*, *Trap* and *c-Fos* are listed in Table 1.

2.4.4. Pit formation assay

100 μ l RAW 264.7 cells were seeded on cortical bovine bone slices (6 mm in diameter, 0.4 μ m in thickness) that provided a smooth mineralised surface at a density of 1×10^4 cells/ml. After 14 days of OCM culture, the resorption area formed by the functional osteoclasts was imaged by SEM. ImageJ software (National Institutes of Health, Bethesda, MD, USA) was used to quantify the total number and area of resorption pits.

2.5. Mechanism exploration

2.5.1. Quantitative RT-PCR

Cells were seeded in 6-well plates at a density of 5×10^4 cells per well. Total cellular RNA was extracted from cells cultured in OM (MC3T3-E1) and OCM (RAW264.7) for 7 days. Subsequent experiments were carried out as described above in 2.3.4. The primer sequences of mouse *Gapdh*, *Axin2*, *Lrp5*, *RANKL* and *RANK* are listed in Table 1.

2.5.2. Western blot analysis

Cells were seeded in 6 cm dishes at a density of 1×10^5 cells per dish. To detect proteins, cells were lysed in a lysis buffer containing 2% protease inhibitor. The protein concentrations were measured using a BCA protein assay kit (Thermo Scientific). An equal amount of protein was subjected to 5% SDS-PAGE and transferred to a polyvinylidene fluoride membrane. For the protein extracted from MC3T3-E1 cells, the membrane was incubated with primary antibodies specific to β -catenin, WNT-3A and GAPDH (Abcam, Cambridge, UK) at 4°C overnight. For the protein extracted from RAW264.7 cells, the membrane was incubated with primary antibodies specific to p65, phospho-p65 (p-p65), I κ B α , phospho-I κ B α (p-I κ B α) and GAPDH (Abcam). Then, the membranes were incubated with peroxidase-conjugated secondary antibodies at room temperature. The enhanced chemiluminescence (ECL) kit (CWBI0, Beijing, China) was used to detect the visualised immunoreactive protein bands.

2.6. Statistical analysis

The results are presented as mean \pm standard deviation. The data were analysed using SPSS 21.0 software (SPSS Inc., Chicago, IL, USA). One-way analysis of variance (ANOVA) was performed for data analysis. A *P* value of <0.05 was considered statistically significant.

3. Results

3.1. Preparation and characterisation of PCL/Zn scaffolds

Fig. 1A showed the appearance of the scaffolds. The colour of the scaffolds deepened with increasing Zn content. The extract concentration of Zn^{2+} (Fig. 1B) reflected the sustained-release trend of Zn in the PCL scaffolds. Fig. 1C showed the structure and surface morphology of the scaffolds. The surfaces were uniform, which indicated that scaffolds with designed structures were obtained. Moreover, the Zn particles were wrapped and evenly distributed in the PCL/Zn scaffolds. The EDS maps and spectra confirmed that Zn element was uniformly distributed in the scaffolds, and the amount of white dots representing Zn element obviously increased with the increase of the mixing ratio of Zn in the composite scaffolds (Fig. 1D). Figure S1 reflected the actual strut diameter, pore size, layer thickness, and porosity of the prepared scaffolds. According to the surface images, the strut diameter and pore size of the scaffolds were close to the theoretical value of 300 μ m. According to the cross-sectional images, the layer thickness of the scaffolds were slightly smaller than the theoretical value of 300 μ m, as under the influence of

gravity, the struts collapsed slightly during the printing process. The cross sections of the struts were oblate (the width was slightly larger than the height), and the porosity values were correspondingly reduced to $43.53 \pm 3.37\%$, which were lower than the theoretical value of 50%. We concluded that the processing accuracy of the scaffolds was acceptable, except that the layer thickness was slightly lower than the theoretical value, and the change of the Zn content had no influence on the overall processing quality of the scaffolds.

In the mechanical test, the elastic modulus of the PCL scaffold was the lowest in both compression and three-point flexure. In the compression test, there was no statistical difference between the PCL-2Zn and PCL-3Zn groups, and they both provided better results than the other groups, while PCL-2Zn was the best-performing group in the three-point flexure test ($P < 0.05$) (Fig. 2A and B). The water-in-air contact angle reflected the hydrophilic/hydrophobic properties of the material surface. The appearance of the samples used for the contact angle measurements as well as their surface morphologies and surface roughness were shown in Figure S2. The results showed that the surfaces we selected as smooth as possible had no difference in roughness among groups ($P < 0.05$), and because the contents of Zn particles were particularly low, and most of them were wrapped in the PCL matrix instead of protruding from the surfaces, they also did not cause general change of the roughness of the PCL. Fig. 2C and D showed that the hydrophilicity of the composite scaffold increased with increasing mixing ratio of Zn ($P < 0.05$). The live/dead assay revealed a large number of green cells (live cells) on the scaffolds, and a small amount of red cells (dead cells) in all groups, indicating that none of these scaffolds had obvious cytotoxicity. Interestingly, the scaffolds in the PCL-2Zn and PCL-3Zn groups showed more live cells attached to the surface than the scaffolds in the PCL and PCL-1Zn groups (Fig. 2E).

3.2. In situ osteogenesis and osteoclastogenesis of scaffolds in vivo

All rats survived the observation period and the surgical wounds showed no visible inflammation. The rats were sacrificed after 8 weeks. All implants were well positioned within the calvaria. Micro-CT reconstruction of the calvaria showed that all the scaffolds groups displayed better bone-promoting effects compared with the blank control group. In the range of 0–2 wt% Zn, the bone-promoting effect of PCL/Zn scaffolds enhanced with increasing Zn content, reaching a maximum in the 2 wt% Zn group. However, when the content of Zn was increased to 3 wt%, the bone-promoting effect decreased, still better than the pure PCL and blank control group (Fig. 3A). The bone mineral density (BMD) and bone volume (BV) calculations indicated similar trend (Fig. 3B and C). H&E staining showed more eosinophilic bone-like tissues in the experimental groups, especially in the PCL-2Zn group, where more bone-like tissues grew along the edge of the defect to the center; and this was confirmed by Masson's trichrome staining (Fig. 3D and E). Following immunohistochemistry staining of OCN, we observed the highest content of dark brown granules around the cytoplasm and nucleus in the PCL-2Zn group (Fig. 3F). The trends for H&E, Masson's trichrome and OCN immunohistochemistry staining were consistent with that of the micro-CT results. In the TRAP-stained sections, we observed that the blank control, PCL and PCL-1Zn groups did not show obvious TRAP-positive cells, while the PCL-2Zn group exhibited scattered osteoclasts, and the PCL-3Zn group showed more TRAP-positive cells on the edge of the cortical bone surrounding the scaffolds (Fig. 3G). Furthermore, the count of TRAP-positive cells confirmed the result (Fig. 3H).

3.3. Zn^{2+} promoted osteogenesis in a dose-dependent manner in vitro

Fig. 4A and B showed that after 1, 3, 5 and 7 days of culture, the 1, 2, 3 and 4 mg/L Zn^{2+} solutions were not cytotoxic to MC3T3-E1 cells.

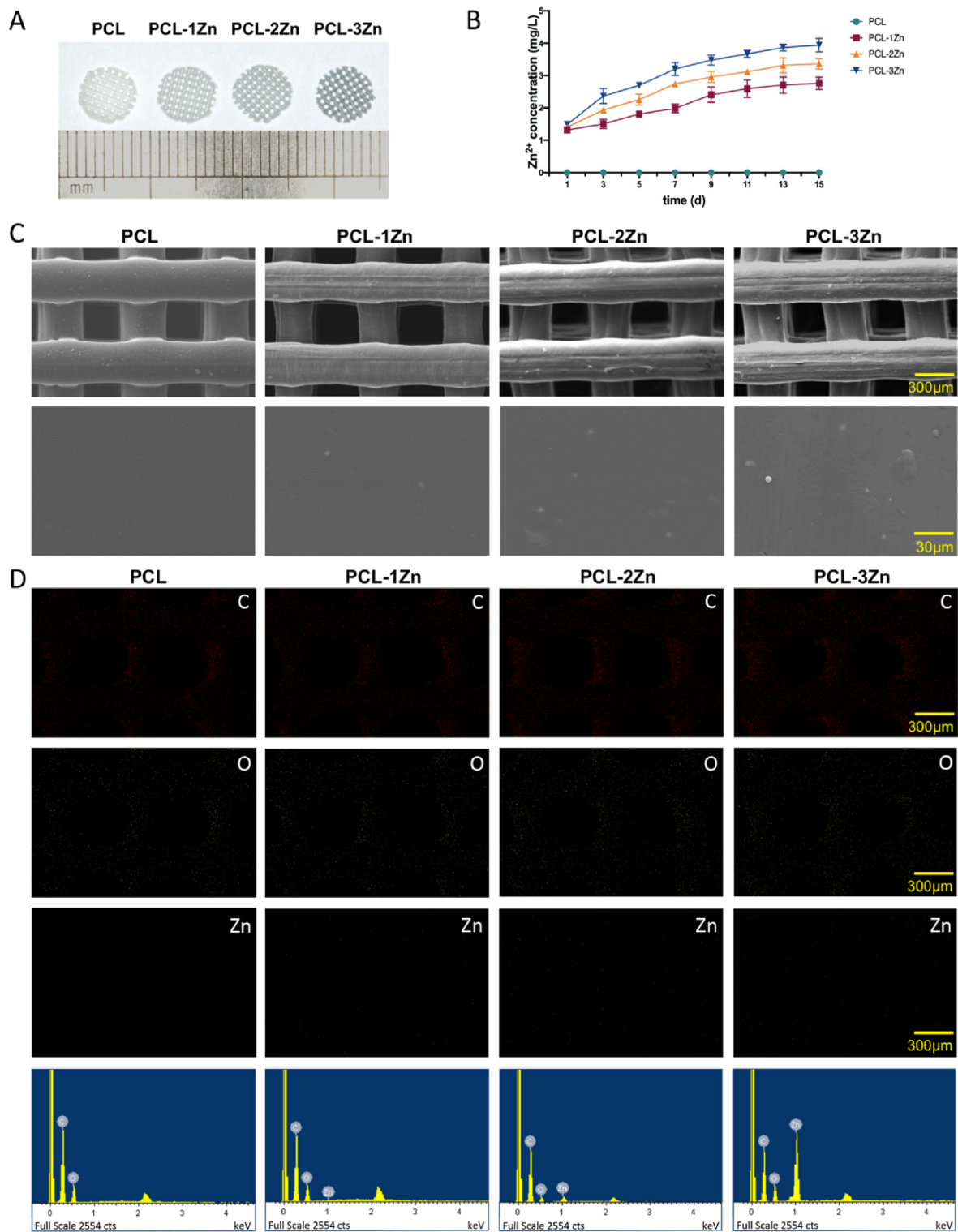


Fig. 1. Characterisation of PCL/Zn scaffolds. (A) General appearance of the scaffolds. (B) Concentration of Zn²⁺ released from the scaffolds on days 1, 3, 5, 7, 9, 11, 13 and 15. (C) Morphologies and structures of the scaffolds (upper row for 50 × , lower row for 500 ×). (D) Energy-dispersive spectrometry analysis of the surface elements.

Moreover, the ALP staining and quantification results showed that Zn²⁺ significantly enhanced osteogenesis compared with the control group, especially in the group with a Zn²⁺ concentration of 1 mg/L ($p < 0.05$) (Fig. 4C and D). Interestingly, as the Zn²⁺ concentration increased in the range of 1–4 mg/L, the bone-promoting effect weakened. Similar trends

were observed in ARS staining and quantification assays (Fig. 4E and F). In the RT-PCR assay, gene expression of osteogenic indicators (*Alp* and *Runx2*) showed a consistent trend after being cultured in OM for 7 days (Fig. 4G and H).

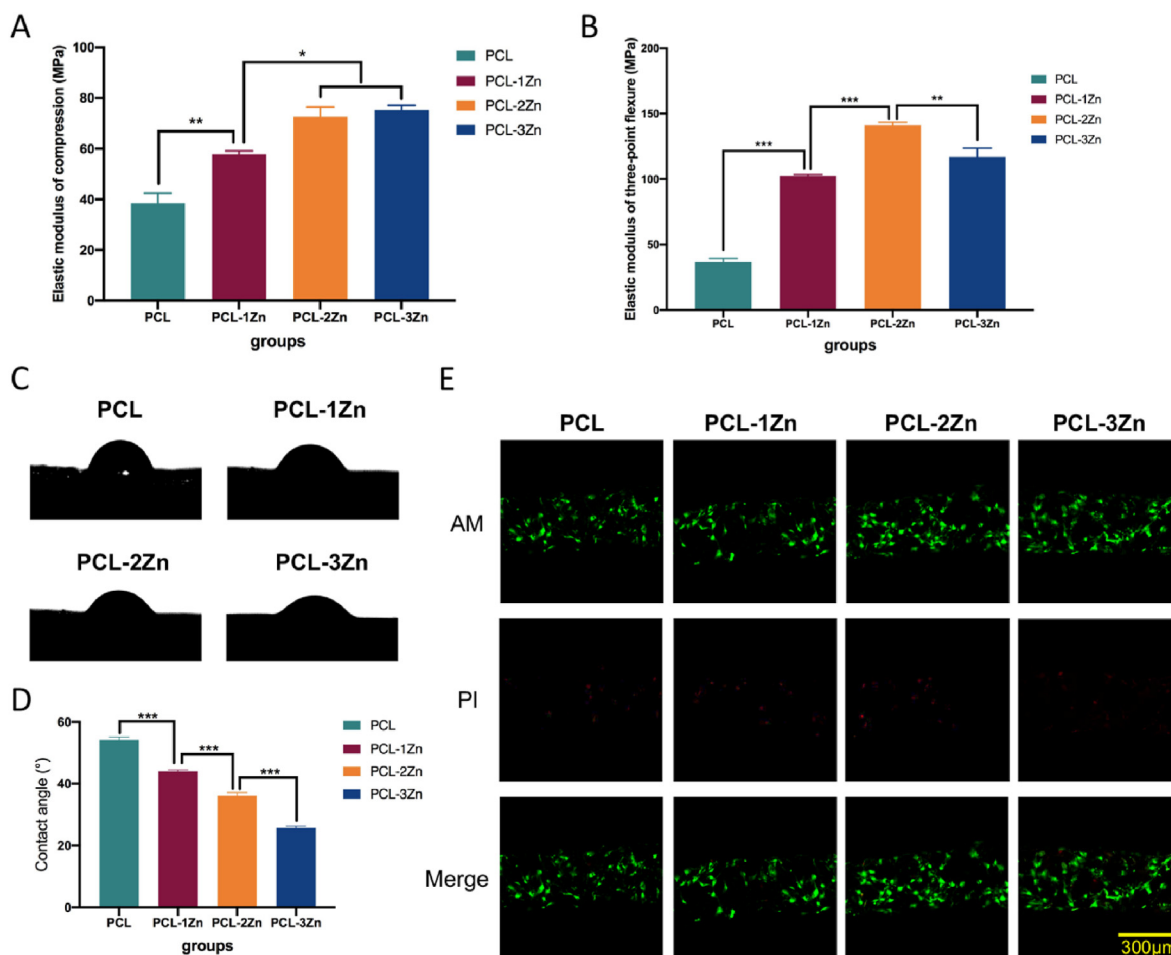


Fig. 2. The mechanical properties, hydrophilicity and cytotoxicity of PCL/Zn scaffolds. (A, B) Elastic moduli of compression and three-point flexure of each group. Mean \pm standard deviation (SD); $n = 5$; * $P < 0.05$, ** $P < 0.01$, *** $P < 0.001$. (C) Water contact angles of each scaffold. (D) Summary of the water contact angle results. Mean \pm SD; $n = 5$; *** $P < 0.001$. (E) Live/dead staining of MC3T3-E1 cells cultured on the scaffolds of each group. Live cells were coloured green and damaged cells were coloured red.

3.4. Zn^{2+} promoted osteoclastogenesis in a dose-dependent manner *in vitro*

Fig. 5A and B showed that after 1, 3, 5 and 7 days of culture, the Zn^{2+} solutions were non-cytotoxic to RAW 264.7 cells. Regarding the formation of mature osteoclasts expressing TRAP, multinucleated TRAP-positive osteoclasts were formed in a concentration-dependent manner (Fig. 5C). In the range of 2–4 mg/L, the volume of osteoclasts gradually increased with increasing Zn^{2+} concentration. However, compared with the control group, the 1 mg/L Zn^{2+} solution had no effect on osteoclast morphology. The TRAP activity assay displayed the same trend (Fig. 5D). Gene expression of osteoclast indices *Trap* and *c-Fos*, was measured 7 days after induction, and the results confirmed the abovementioned trend (Fig. 5E and F). Mature osteoclasts form absorption pits on cortical bovine bone slices and, after 14 days, an increase in the percentage and area of absorption pits were also noticed, again in a concentration-dependent manner (Fig. 5G, H and 5I).

3.5. Zn^{2+} regulated osteogenesis and osteoclastogenesis via Wnt/ β -catenin and NF- κ B signalling pathways

To determine whether the Wnt signalling pathway was involved in the regulation of osteogenic differentiation by Zn^{2+} , RT-PCR and Western blot analyses were carried out after 7 days of osteogenic induction. Fig. 6A and B shows that the expression of *Axin2* and *Lrp5* had the same

trend as *in vitro* osteogenic indicators. To analyse the protein expression of key molecules in the Wnt/ β -catenin pathway, β -catenin and WNT-3A expression level were detected; the results showed that these molecules increased in the same dose-dependent manner (Fig. 6C).

To explore the mechanism of action of Zn^{2+} in osteoclastogenesis, activation of the NF- κ B pathway was also analysed by RT-PCR and Western blot analysis. Fig. 6D and E showed that gene expression levels of *RANKL* and *RANK* were dose-dependent, and the trend was the same as for *in vitro* osteoclast indicators; this was confirmed by the expression of p-p65 and p-I κ B α in the Western blot analysis (Fig. 6F).

The above results indicated that Zn^{2+} regulated osteogenesis and osteoclastogenesis through the activation of Wnt/ β -catenin and NF- κ B signalling pathway.

4. Discussion

PCL is one of the most important thermoplastic polymers in BTE, and has attracted considerable attention due to its biocompatibility, biodegradability and adaptability [32]. In addition, by using 3D printing technology, its shape, porosity and mechanical properties can be well defined and controlled [33]. However, when used alone, insufficient osteogenic ability and mechanical strength limit its application. To improve its physical and biological properties, previous studies mixed PCL with inorganic particles. These composite materials exploit the advantages of each

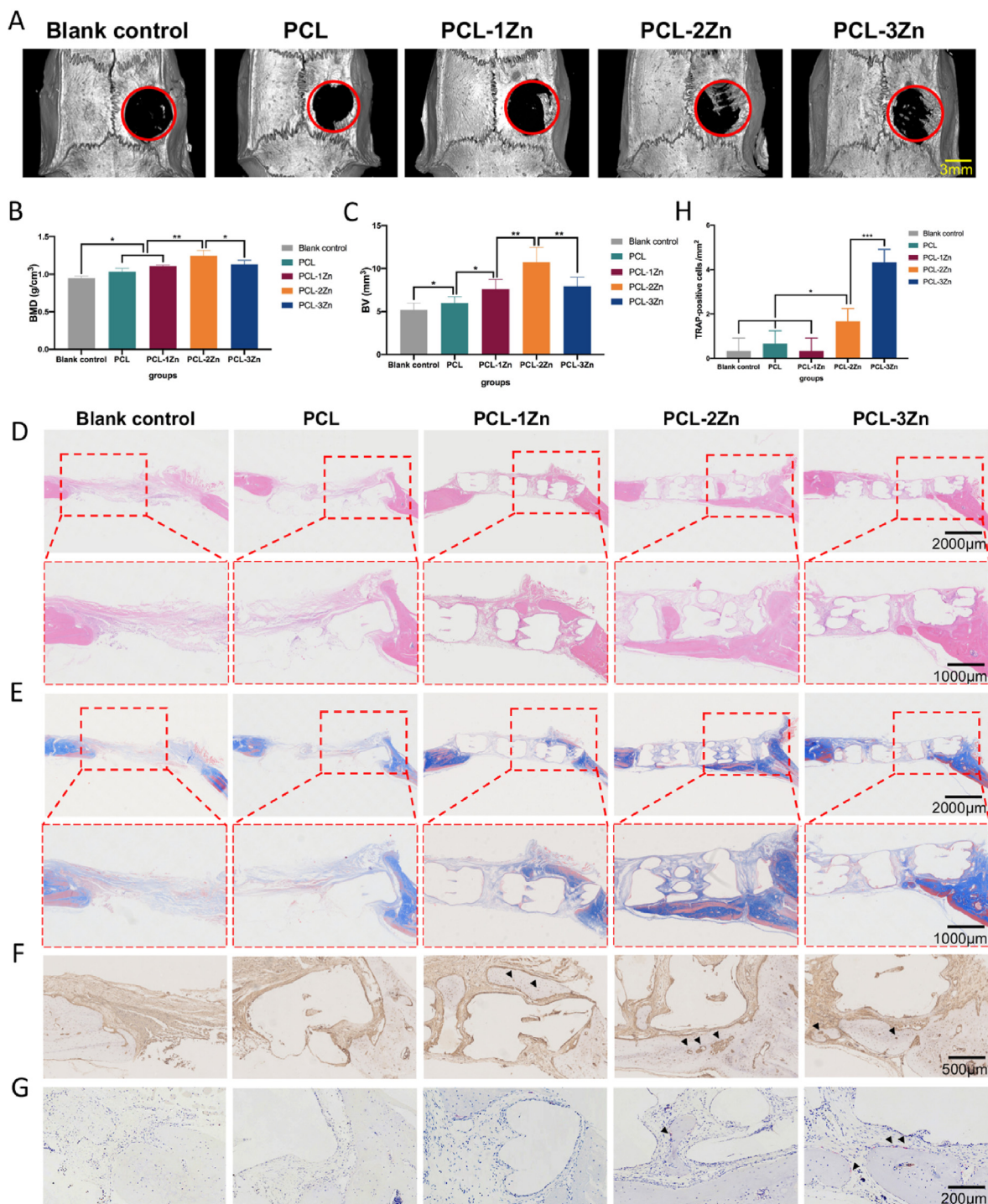


Fig. 3. The bone formation-promoting effect of Zn *in vivo* was related to its content. (A) Micro-computed tomography images of the calvaria of Sprague–Dawley rats. (B, C) Quantitative analysis of bone mineral density (BMD) and bone volume (BV). Mean \pm standard deviation (SD); n = 6; * P < 0.05, *** P < 0.01. (D, E) H&E and Masson's trichrome staining of calvaria defects at 8 weeks after surgery. (F) OCN immunohistochemical staining of calvaria defects at 8 weeks after surgery. Arrow: Dark brown granules in the cytoplasm and around the nuclei. (G) TRAP staining of calvaria defects at 8 weeks after surgery. Arrow: TRAP-positive cells. (H) Number of TRAP-positive cells per mm². Mean \pm SD; n = 6; * P < 0.05, *** P < 0.001.

component, such as easy processing, adaptability, strength and biological effects [34]. Although previous studies have successfully introduced Zn into polymer scaffolds, they use Zn-containing compounds such as ZnO coating [62] or zinc-doped HA [63] instead of high-purity Zn alloy particles as we did. In addition, most of the Zn-containing scaffolds have only

been studied the osteogenic properties, without the exploration of the influence of Zn content on osteoclastogenesis.

Zinc is known as the “calcium” of the 21st century because it plays many important biological roles in the body, including promoting matrix mineralisation, stimulating new bone formation and maintaining bone

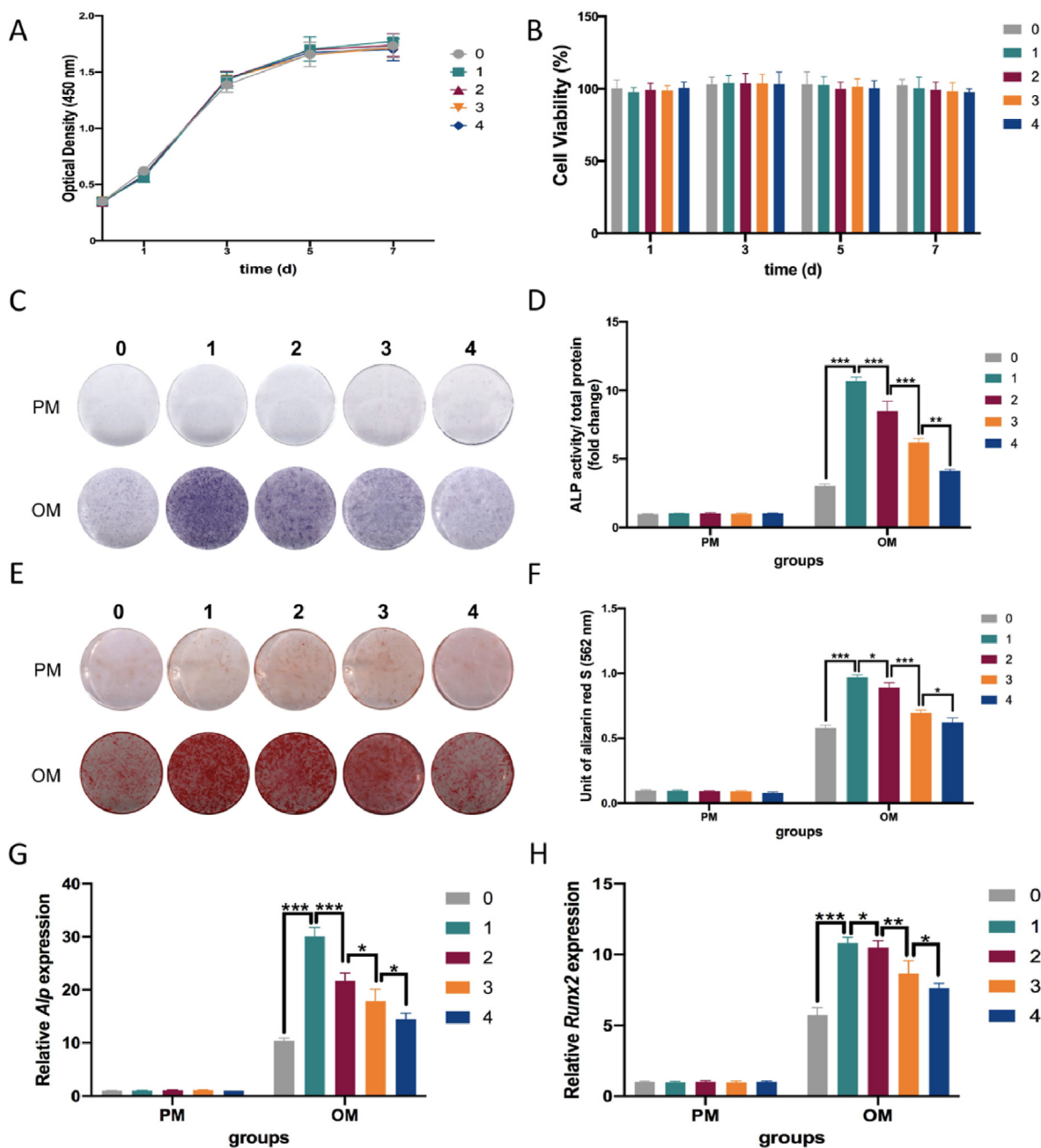


Fig. 4. Zn^{2+} promoted osteogenic differentiation of MC3T3-E1 cells *in vitro* in a dose-dependent manner. (A, B) Proliferation curves and cell viability of MC3T3-E1 cells cultured with Zn^{2+} solutions of 1, 2, 3 and 4 mg/L compared with proliferation medium. Mean \pm standard deviation (SD); $n = 3$. (C, D) ALP staining and quantification of ALP activity of MC3T3-E1 cells cultured with Zn^{2+} solutions 7 days after osteogenic induction (OI). Mean \pm SD; $n = 3$; $**P < 0.01$, $***P < 0.001$. (E, F) ARS staining and quantification of the mineralisation of MC3T3-E1 cells cultured for 14 days after OI. Mean \pm SD; $n = 3$; $*P < 0.05$, $***P < 0.001$. (G, H) Expression of osteogenic genes *Alp* and *Runx2* in MC3T3-E1 cells cultured for 7 days after OI. Mean \pm SD; $n = 3$; $*P < 0.05$, $**P < 0.01$, $***P < 0.001$.

mass[35]. Besides, our previous study have confirmed the osteogenic ability of pure zinc [37]. What's more, Zn alloys hold favourable mechanical strength, degradation rates [21]. Therefore, incorporating Zn powder into the PCL scaffold may be a feasible method to improve the osteogenesis and mechanical properties of PCL. Herein, we fabricated PCL/Zn scaffolds with Zn powder content of 1, 2 and 3 wt%. We found that the incorporation of Zn powder improved mechanical properties of PCL, PCL scaffolds with 2 wt% and 3 wt% of Zn had the best compression strength (72.6 ± 2.75 and 75.35 ± 1.22 MPa, respectively), while the 2 wt% experimental group had the best three-point flexural strength (141.15 ± 1.66 MPa). This may be because the Zn powder enhanced the

mechanical properties of the composite scaffolds, although excessive Zn particles affected the integrity of the PCL fibre. Previous study of Dong et al. has pointed out that properly incorporated Mg micro-particles of 26.8 μm enhanced the mechanical properties of PCL scaffolds, but due to the local enrichment of micro-particles in the PCL matrix, excessive particles weakened the mechanical enhancement [38]. However, Adhikari et al. indicated that Mg particles of 325 mesh decreased the ultimate tensile strength and Young's modulus of the PCL matrix. When the polymer deformed, it would produce an elastic response, but the presence of particles would cause a local and diffuse inelastic process. Besides, the elongation force changed the crystalline phase in PCL, and the presence of

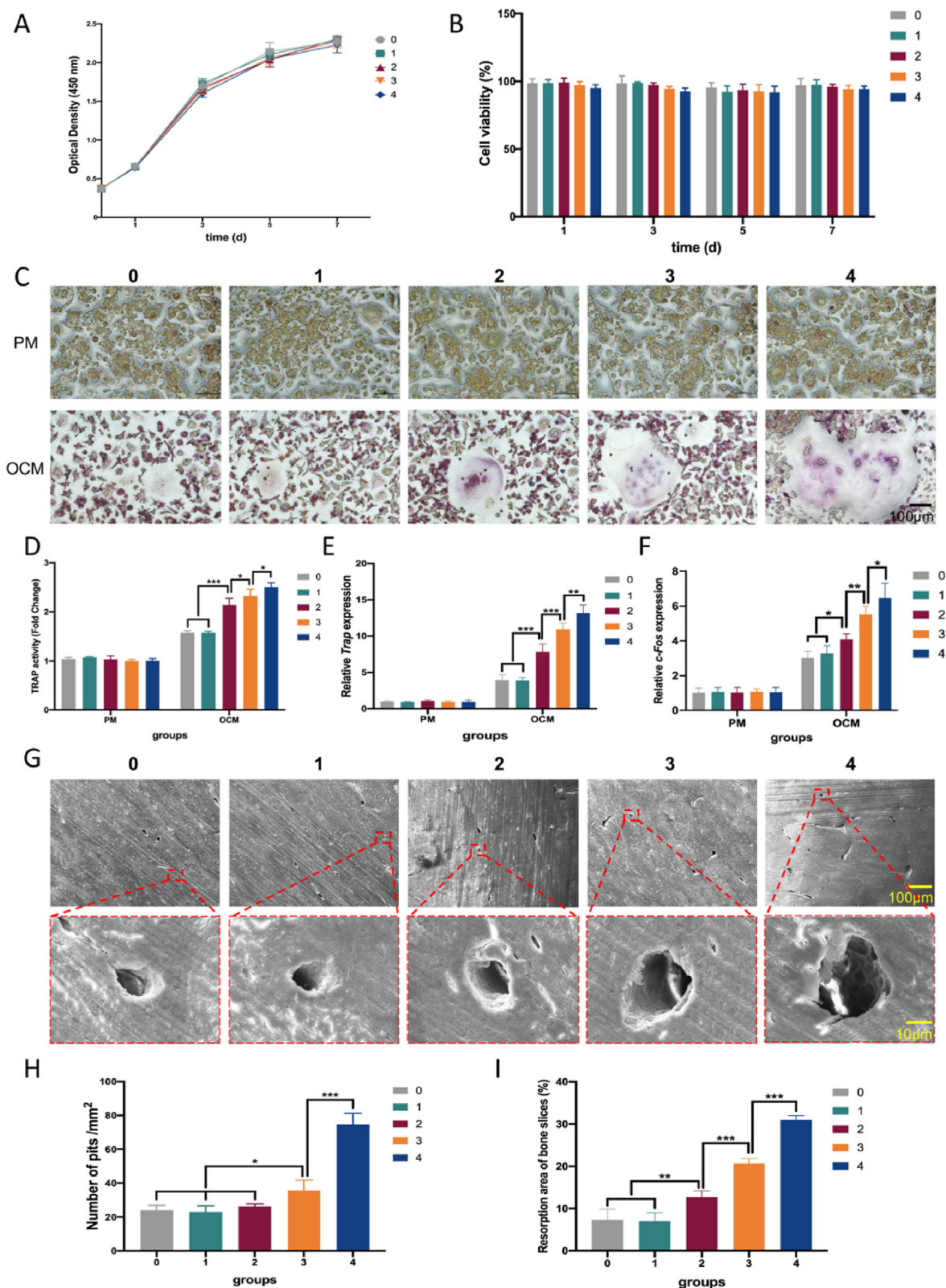


Fig. 5. Zn²⁺ affected the osteoclastogenesis of RAW264.7 cells *in vitro* in a dose-dependent manner. (A, B) Proliferation curves and cell viability of RAW264.7 cells cultured with Zn²⁺ solutions of 1, 2, 3 and 4 mg/L compared with proliferation medium. Mean ± standard deviation (SD); n = 3. (C, D) TRAP staining and quantification of the TRAP activity of RAW264.7 cells cultured with Zn²⁺ solutions after induction for 7 days. Mean ± SD; n = 3; *p < 0.05, ***p < 0.001. (E, F) Expression of osteoclast-related genes *Trap* and *c-Fos* in RAW264.7 cells cultured for 7 days after induction. Mean ± SD; n = 3; *p < 0.05, **p < 0.01, ***p < 0.001. (G, H, I) Pit formation (upper row for 100 ×, lower row for 1000 ×) and quantification thereof on cortical bovine bone slices cultured with Zn²⁺ solutions after induction for 14 days. Mean ± SD; n = 3; *p < 0.05, **p < 0.01, ***p < 0.001.

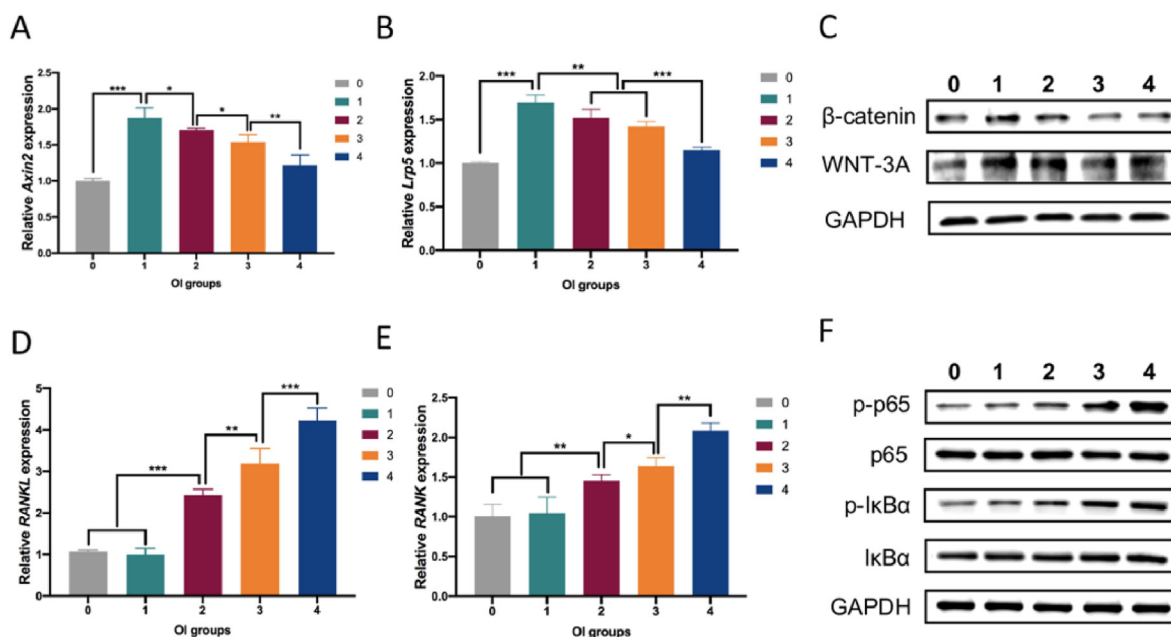


Fig. 6. Zinc acted on the osteogenesis and osteoclastogenesis processes through the Wnt/ β -catenin and NF- κ B pathways. (A, B) Expression of genes *Axin2* and *Lrp5* in MC3T3-E1 cells cultured for 7 days after induction. Mean \pm standard deviation (SD); $n = 3$; * $p < 0.05$, ** $p < 0.01$, *** $p < 0.001$. (C) β -catenin and WNT-3A expression detected by Western blot analysis. (D, E) Expression of genes *RANKL* and *RANK* in RAW264.7 cells cultured for 7 days after induction. Mean \pm SD; $n = 3$; * $p < 0.05$, ** $p < 0.01$, *** $p < 0.001$. (F) p-p65, p65, p-I κ B α and I κ B α expression detected by Western blot analysis.

particles could interfere with this crystallinity, thereby affecting mechanical properties [39].

PCL is usually regarded as hydrophobic because it lacks cell recognition signals and biological adhesion sites [42]. The contact angle measurements showed that the hydrophilicity of the scaffold surface increased with increasing Zn content. Similar to the result we reached, Zhao et al. mixed different content of Mg particles into the PCL matrix [43]. Their results showed that as the content of Mg particles increased, the hydrophilicity of the PCL composite material increased. This may be attributed to the presence of inorganic metal materials on the film surface that are more hydrophilic than pure PCL, and the metal powder changed the melting and solidification conditions of PCL, causing changes to the PCL surface structure during extrusion and molding. Live/dead staining established that, though no scaffolds had obvious cytotoxicity, for those containing 2 wt% and 3 wt% Zn had more cell adhesion onto the surfaces, which was in consistent with hydrophilicity results.

From the *in vivo* experiments, all of the scaffold-containing groups showed more osteogenic effects than that of the blank control group. Moreover, when 2 wt% Zn was mixed in the PCL scaffolds, the bone-promoting effect was strongest. However, when the concentration of Zn was increased to 3 wt%, the osteoclasts at the edge of the new bone tissue around the scaffold began to increase significantly, and the amount of new bone started to decrease. Although there was no obvious osteoclast staining in the new bone tissue around the scaffolds containing 1 wt% Zn, the amount of new bone was less than that of the 2 wt% Zn group. This was likely because the Zn content had not reached its optimal value. Correspondingly, there was even less new bone formation around the pure PCL scaffolds. Based on the *in vitro* and *in vivo* studies, we concluded that the best mechanical and osteogenic properties were obtained when 2 wt% Zn was mixed into the PCL scaffolds.

Previous studies noted that Zn stimulates cell proliferation and differentiation, as well as protein synthesis, in MC3T3-E1 cells. Togari et al. reported that adding 10 μ M Zn to MC3T3-E1 medium increased ALP expression [27]. In addition, Zn²⁺ can act as an activator or co-activator of runt-related transcription factor 2 (RUNX2) [44,45]. Other studies have shown that free extracellular Zn²⁺ may be deposited on bone formation sites of osteoblasts or osteocytes, which suggests that it

participates in processes related to bone matrix synthesis [46,47]. However, O'Connor JP et al. pointed out that the positive effect of Zn²⁺ on osteoblast activity occurs within a narrow dose range (1–50 μ M), doses exceeding 50 μ M inhibit osteogenic activity [27]. Moreover, Togari et al. noted that treating MC3T3-E1 cultures with high Zn²⁺ doses (50 and 100 μ M) could inhibit calcium deposition, which means that it may be unreasonable to discuss the role of Zn in the process of osteogenesis without the dose [48].

Excessive activation of osteoclasts in the initial stage of implantation may delay the healing of bone tissue, as they absorb existing bone tissue [49,50]. Zn is also necessary for osteoclastogenesis, as an essential trace metal. However, there is still no consensus concerning the relationship between Zn and osteoclastogenesis. Hie et al. found that when 5-week-old female Wistar rats were fed a Zn-free diet, the number of osteoclasts observed in their distal femoral growth plate was 50% less than that of control rats (normal diet). Also, bone extract from Zn-starved rats exhibited reduced TRAP activity [51]. Besides, Hadley et al. observed increased TRAP activity in rats fed extra amounts of zinc (2.5–30 mg zinc per kg of chow) [52]. Similar to the trend of our *in vivo* results, which indicated that high Zn content may cause increased osteoclast activity, Kawamura et al. fabricated Zn-tricalcium phosphate/hydroxyapatite (ZnTCP/HAP) implants and implanted them in the femora of New Zealand White rabbits, and found that there was significant new bone formation around the ZnTCP/HAP implants of 0.316 Zn wt%, however, an increased bone resorption was observed on the endosteal surface around the ZnTCP/HAP implants of 0.633 Zn wt% [53]. In contrast, some *in vitro* studies found that sub-nanomolar concentrations of exogenous Zn inhibited osteoclastogenesis [54,55].

Our subsequent *in vitro* experiments showed that the osteogenic and osteoclastic effect of Zn was dose-dependent. In the range of 1–4 mg/L, Zn²⁺ ions promoted osteogenic differentiation of MC3T3-E1 cells and a Zn²⁺ concentration of 1 mg/L had the best bone-promoting effect. The effect lessened with increasing concentration. On the other hand, in the range of 1–4 mg/L, Zn²⁺ concentrations of 2, 3 and 4 mg/L promoted osteoclastogenesis of RAW264.7 cells, and this effect was enhanced with increasing concentration. The Zn²⁺ concentration of 1 mg/L did not show a significant effect compared with the control group. These results are

consistent with those of *in vivo* experiments, i.e. Zn promoted osteogenesis in a dose-dependent manner, and the optimal concentration of Zn to promote bone formation peaked within a certain range. Furthermore, within a certain concentration range, Zn had no significant effect on the activity and number of osteoclasts. However, when it exceeded this range, osteoclastogenesis was promoted.

The Wnt/ β -catenin pathway plays a key role in the process of osteogenic differentiation [56]. *Lrp5* is a canonical Wnt co-receptor and *Axin2* is a direct target of Wnt activation [57,58]. Moreover, activation of the Wnt/ β -catenin signalling pathway is reflected in the accumulation of β -catenin in the presence of WNT protein. In our study, significant changes were seen in the expression levels of the Wnt/ β -catenin pathway-specific genes *Axin2* and *Lrp5*, and the proteins β -catenin and WNT-3A. Thus, the effect of Zn^{2+} on the osteogenesis of MC3T3-E1 cells was related to the activation of this signalling pathway.

Binding of RANKL to its receptor RANK activates the NF- κ B signalling pathway, inducing osteoclast differentiation [59]. I κ B α is an important regulatory protein that inhibits NF- κ B signalling. Previous studies have shown that, when phosphorylated, free p-I κ B was ubiquitinated, while p65 was activated. Subsequently, p-p65 entered the nucleus and activated specific transcription factors [60,61]. In our study, Zn^{2+} simultaneously promoted the expression of p-I κ B α and p-p65, while the osteoclast-specific genes *RANKL* and *RANK* were upregulated, indicating that NF- κ B signalling was activated during the process of osteoclastogenesis. Our results demonstrated that activation of the NF- κ B pathway was a potential mechanism underlying the osteoclastogenesis induced by Zn^{2+} .

5. Conclusion

We incorporated Zn into PCL scaffolds to achieve PCL/Zn composite scaffolds, and found that the scaffold containing 2 wt% Zn was optimal for bone regeneration and show great application potential. Moreover, the role of Zn in the processes of osteogenesis and osteoclastogenesis was related to the Wnt/ β -catenin and NF- κ B signalling pathways, respectively. This study provides new insight into the role that Zn plays in the process of bone regeneration and endows composite materials with biological functions.

Data availability

All experimental data within the article are available from the corresponding author upon reasonable request.

Credit author statement

Siyi Wang and Dandan Xia provided the concept of this research, conducted experimental design and completed most of the experiments; Ranli Gu and Feilong Wang completed data sorting and analysis work; Xiao Zhao, Fan Yang and Yuqian Xu framed the figures and wrote the original draft of the article; Fanyu Yan and Yuan Zhu refined the entire manuscript; Yunsong Liu supervised the whole study and obtained funding support for this research.

Declaration of competing interest

The authors declare that they have no known competing financial interests or personal relationships that could have appeared to influence the work reported in this paper.

Acknowledgment

This study was supported by the National Natural Science Foundation of China [grant numbers 82170929, 81970908, 51901003 and 81771039] and the Beijing Natural Science Foundation [L212014].

Appendix A. Supplementary data

Supplementary data to this article can be found online at <https://doi.org/10.1016/j.mtbio.2021.100202>.

References

- [1] U. Kneser, D.J. Schaefer, E. Polykandriotis, R.E. Horch, Tissue engineering of bone: the reconstructive surgeon's point of view, *J. Cell Mol. Med.* 10 (1) (2006) 7–19.
- [2] D. Tang, R.S. Tare, L.Y. Yang, D.F. Williams, K.L. Ou, R.O. Oreffo, Biofabrication of bone tissue: approaches, challenges and translation for bone regeneration, *Biomaterials* 83 (2016) 363–382.
- [3] T. Winkler, F.A. Sass, G.N. Duda, K. Schmidt-Bleek, A review of biomaterials in bone defect healing, remaining shortcomings and future opportunities for bone tissue engineering: the unsolved challenge, *Bone Joint Res.* 7 (3) (2018) 232–243.
- [4] H.C. Pape, A. Evans, P. Kobbe, Autologous bone graft: properties and techniques, *J. Orthop. Trauma.* 24 Suppl 1 (2010) S36–40.
- [5] A.R. Amini, C.T. Laurencin, S.P. Nukavarapu, Bone tissue engineering: recent advances and challenges, *Crit. Rev. Biomed. Eng.* 40 (5) (2012) 363–408.
- [6] S.N. Khan, F.P. Cammisa Jr., H.S. Sandhu, A.D. Diwan, F.P. Girardi, J.M. Lane, The biology of bone grafting, *J. Am. Acad. Orthop. Surg.* 13 (1) (2005) 77–86.
- [7] S. Kashte, A.K. Jaiswal, S. Kadam, Artificial bone via bone tissue engineering: current scenario and challenges, *Tissue Eng. Regen. Med.* 14 (1) (2017) 1–14.
- [8] S. Bose, M. Roy, A. Bandyopadhyay, Recent advances in bone tissue engineering scaffolds, *Trends Biotechnol.* 30 (10) (2012) 546–554.
- [9] S.J. Hollister, Porous scaffold design for tissue engineering, *Nat. Mater.* 4 (7) (2005) 518–524.
- [10] H.T. Liao, Y.Y. Chen, Y.T. Lai, M.F. Hsieh, C.P. Jiang, The osteogenesis of bone marrow stem cells on mPEG-PCL-mPEG/hydroxyapatite composite scaffold via solid freeform fabrication, *BioMed Res. Int.* 2014 (2014) 321549.
- [11] Y. Qin, P. Wen, H. Guo, D. Xia, Y. Zheng, L. Jauer, R. Poprawe, M. Voshage, J.H. Schleifenbaum, Additive manufacturing of biodegradable metals: Current research status and future perspectives, *Acta Biomater.* 98 (2019) 3–22.
- [12] L. Rosetti, V. Parisi, M. Petretta, C. Cavallo, G. Desando, I. Bartolotti, B. Grigolo, Scaffolds for bone tissue engineering: state of the art and new perspectives, *Mater. Sci. Eng. C Mater. Biol. Appl.* 78 (2017) 1246–1262.
- [13] J. Babilotte, V. Guduric, D. Le Nihouannen, A. Naveau, J.C. Fricain, S. Catros, 3D printed polymer-mineral composite biomaterials for bone tissue engineering: fabrication and characterization, *J. Biomed. Mater. Res. B Appl. Biomater.* 107 (8) (2019) 2579–2595.
- [14] Liu B. Kenry, Recent advances in biodegradable conducting polymers and their biomedical applications, *Biomacromolecules* 19 (6) (2018) 1783–1803.
- [15] S. Wang, R. Li, D. Xia, X. Zhao, Y. Zhu, R. Gu, J. Yoon, Y. Liu, The impact of Zn-doped synthetic polymer materials on bone regeneration: a systematic review, *Stem Cell Res. Ther.* 12 (1) (2021) 123.
- [16] K. Khoshroo, T.S. Jafarzadeh Kashi, F. Moztafzadeh, M. Tahriri, H.E. Jazayeri, L. Tayebi, Development of 3D PCL microsphere/TiO₂ nanotube composite scaffolds for bone tissue engineering, *Mater. Sci. Eng. C Mater. Biol. Appl.* 70 (Pt 1) (2017) 586–598.
- [17] H. Kabir, K. Munir, C. Wen, Y. Li, Recent research and progress of biodegradable zinc alloys and composites for biomedical applications: biomechanical and biocorrosion perspectives, *Bioact Mater* 6 (3) (2021) 836–879.
- [18] Y. Zheng, X. Gu, F. Witte, Biodegradable metals, *Materials Science & Engineering R-Reports* 77 (2014) 1–34, e2000900.
- [19] G. Li, H. Yang, Y. Zheng, X.H. Chen, J.A. Yang, D. Zhu, L. Ruan, K. Takashima, Challenges in the use of zinc and its alloys as biodegradable metals: perspective from biomechanical compatibility, *Acta Biomater.* 97 (2019) 23–45.
- [20] B. Jia, H. Yang, Y. Han, Z. Zhang, X. Qu, Y. Zhuang, Q. Wu, Y. Zheng, K. Dai, In vitro and in vivo studies of Zn-Mn biodegradable metals designed for orthopedic applications, *Acta Biomater.* 108 (2020) 358–372.
- [21] Y. Xu, Q. Liu, B. Dou, B. Wright, J. Wang, Y. Pang, Zn(2+) binding-enabled excited state intramolecular proton transfer: a step toward new near-infrared fluorescent probes for imaging applications, *Adv. Health Mater.* 1 (4) (2012) 485–492.
- [22] G. Meng, X. Wu, R. Yao, J. He, W. Yao, F. Wu, Effect of zinc substitution in hydroxyapatite coating on osteoblast and osteoclast differentiation under osteoblast/osteoclast co-culture, *Regen. Biomater.* 6 (6) (2019) 349–359.
- [23] A.S. Tiffany, D.L. Gray, T.J. Woods, K. Subedi, B.A.C. Harley, The inclusion of zinc into mineralized collagen scaffolds for craniofacial bone repair applications, *Acta Biomater.* 93 (2019) 86–96.
- [24] X. Fu, Y. Li, T. Huang, Z. Yu, K. Ma, M. Yang, Q. Liu, H. Pan, H. Wang, J. Wang, M. Guan, Runx2/Osterix and zinc uptake synergize to orchestrate osteogenic differentiation and citrate containing bone apatite formation, *Adv. Sci.* 5 (4) (2018) 1700755.
- [25] J.P. O'Connor, D. Kanjilal, M. Teitelbaum, S.S. Lin, J.A. Cottrell, Zinc as a therapeutic agent in bone regeneration, *Materials* 13 (10) (2020).
- [26] Y. Yamada, A. Ito, H. Kojima, M. Sakane, S. Miyakawa, T. Uemura, R.Z. LeGeros, Inhibitory effect of Zn²⁺ in zinc-containing beta-tricalcium phosphate on resorbing activity of mature osteoclasts, *J. Biomed. Mater. Res.* 84 (2) (2008) 344–352.
- [27] M. Roy, G. Fielding, A. Bandyopadhyay, S. Bose, Effects of zinc and strontium substitution in tricalcium phosphate on osteoclast differentiation and resorption, *Biomater. Sci.* 1 (1) (2013).
- [28] B.S. Moonga, D.W. Dempster, Zinc is a potent inhibitor of osteoclastic bone resorption in vitro, *J. Bone Miner. Res.* 10 (3) (1995) 453–457.

- [31] W.R. Holloway, F.M. Collier, R.E. Herbst, J.M. Hodge, G.C. Nicholson, Osteoblast-mediated effects of zinc on isolated rat osteoclasts: inhibition of bone resorption and enhancement of osteoclast number, *Bone* 19 (2) (1996) 137–142.
- [32] J.Y. Liu, Fabrication and characterization of polycaprolactone/calcium sulfate whisker composites, *Express Polym. Lett.* 5 (8) (2011) 742–752.
- [33] Y. Rotbaum, C. Puiu, D. Rittel, M. Domingos, Quasi-static and dynamic in vitro mechanical response of 3D printed scaffolds with tailored pore size and architectures, *Mater Sci Eng C Mater Biol Appl.* 96 (2019) 176–182.
- [34] Z. Heydari, D. Mohebbi-Kalhari, M.S. Afarani, Engineered electrospun polycaprolactone (PCL)/octacalcium phosphate (OCP) scaffold for bone tissue engineering, *Mater Sci Eng C Mater Biol Appl.* 81 (2017) 127–132.
- [35] L.M. Plum, L. Rink, H. Haase, The essential toxin: impact of zinc on human health, *Int. J. Environ. Res. Publ. Health* 7 (4) (2010) 1342–1365.
- [36] H. Guo, D. Xia, Y. Zheng, Y. Zhu, Y. Liu, Y. Zhou, A pure zinc membrane with degradability and osteogenesis promotion for guided bone regeneration: In vitro and in vivo studies, *Acta Biomater* 106 (2020) 396–409.
- [37] Q. Dong, M. Zhang, X. Zhou, Y. Shao, J. Li, L. Wang, C. Chu, F. Xue, Q. Yao, J. Bai, 3D-printed Mg-incorporated PCL-based scaffolds: a promising approach for bone healing, *Mater. Sci. Eng. C Mater. Biol. Appl.* 129 (2021) 112372.
- [38] U. Adhikari, X. An, N. Rijal, T. Hopkins, S. Khanal, T. Chavez, R. Tatu, J. Sankar, K.J. Little, D.B. Hom, N. Bhattarai, S.K. Pixley, Embedding magnesium metallic particles in polycaprolactone nanofiber mesh improves applicability for biomedical applications, *Acta Biomater.* 98 (2019) 215–234.
- [39] G. Ciardelli, V. Chiono, G. Vozzi, M. Pracella, P. Giusti, Blends of poly(ϵ -caprolactone) and polysaccharides in tissue engineering applications, *Biomacromolecules* 6 (4) (2005) 1961–1976.
- [40] S. Zhao, K. Xie, Y. Guo, J. Tan, J. Wu, Y. Yang, P. Fu, L. Wang, W. Jiang, Y. Hao, Fabrication and biological activity of 3D-printed polycaprolactone/magnesium porous scaffolds for critical size bone defect repair, *ACS Biomater. Sci. Eng.* 6 (9) (2020) 5120–5131.
- [41] H.R. Kang, C.J. da Costa Fernandes, R.A. da Silva, V.R.L. Constantino, I.H.J. Koh, W.F. Zambuzzi, Mg-Al and Zn-Al layered double hydroxides promote dynamic expression of marker genes in osteogenic differentiation by modulating mitogen-activated protein kinases, *Adv. Health Mater.* 7 (4) (2018).
- [42] M. Yamaguchi, M. Goto, S. Uchiyama, T. Nakagawa, Effect of zinc on gene expression in osteoblastic MC3T3-E1 cells: enhancement of Runx2, OPG, and regucalcin mRNA expressions, *Mol. Cell. Biochem.* 312 (1–2) (2008) 157–166.
- [43] M.H. Fernandes, M.M. Alves, M. Cebotarenco, I.A.C. Ribeiro, L. Grenho, P.S. Gomes, M.J. Carneim, C.F. Santos, Citrate zinc hydroxyapatite nanorods with enhanced cytocompatibility and osteogenesis for bone regeneration, *Mater. Sci. Eng. C Mater. Biol. Appl.* 115 (2020) 111147.
- [44] N. Levaot, M. Hershinkel, How cellular Zn(2+) signaling drives physiological functions, *Cell Calcium* 75 (2018) 53–63.
- [45] A. Togari, S. Arakawa, M. Arai, S. Matsumoto, Alteration of in vitro bone metabolism and tooth formation by zinc, *Gen. Pharmacol.* 24 (5) (1993) 1133–1140.
- [46] S.K. Lee, C.M. Han, W. Park, I.H. Kim, Y.K. Joung, D.K. Han, Synergistically enhanced osteoconductivity and anti-inflammation of PLGA/ β -TCP/Mg(OH)₂ composite for orthopedic applications, *Mater. Sci. Eng. C Mater. Biol. Appl.* 94 (2019) 65–75.
- [47] J.F. Charles, A.O. Aliprantis, Osteoclasts: more than 'bone eaters', *Trends Mol. Med.* 20 (8) (2014) 449–459.
- [48] M. Hie, N. Iitsuka, T. Otsuka, A. Nakanishi, I. Tsukamoto, Zinc deficiency decreases osteoblasts and osteoclasts associated with the reduced expression of Runx2 and RANK, *Bone* 49 (6) (2011) 1152–1159.
- [49] K.B. Hadley, S.M. Newman, J.R. Hunt, Dietary zinc reduces osteoclast resorption activities and increases markers of osteoblast differentiation, matrix maturation, and mineralization in the long bones of growing rats, *J. Nutr. Biochem.* 21 (4) (2010) 297–303.
- [50] H. Kawamura, A. Ito, S. Miyakawa, P. Layrolle, K. Ojima, N. Ichinose, T. Tateishi, Stimulatory effect of zinc-releasing calcium phosphate implant on bone formation in rabbit femora, *J. Biomed. Mater. Res.* 50 (2) (2000) 184–190.
- [51] M. Yamaguchi, M.N. Weitzmann, Zinc stimulates osteoblastogenesis and suppresses osteoclastogenesis by antagonizing NF- κ B activation, *Mol. Cell. Biochem.* 355 (1–2) (2011) 179–186.
- [52] M. Hie, I. Tsukamoto, Administration of zinc inhibits osteoclastogenesis through the suppression of RANK expression in bone, *Eur. J. Pharmacol.* 668 (1–2) (2011) 140–146.
- [53] K.S. Houshyar, C. Tapking, M.R. Borrelli, D. Popp, D. Duscher, Z.N. Maan, M.P. Chelliah, J. Li, K. Harati, C. Wallner, S. Rein, D. Pörringer, G. Reumuth, G. Grieb, S. Mouraret, M. Dadrás, J.M. Wagner, J.Y. Cha, F. Siemers, M. Lehnhardt, B. Behr, Wnt pathway in bone repair and regeneration - what do we know so far, *Front. Cell Dev. Biol.* 6 (2018) 170.
- [54] A. Sebastian, N.R. Hum, D.K. Muruges, S. Hatsell, A.N. Economides, G.G. Loots, Wnt co-receptors Lrp5 and Lrp6 differentially mediate Wnt3a signaling in osteoblasts, *PLoS One* 12 (11) (2017), e0188264.
- [55] Y. Yan, D. Tang, M. Chen, J. Huang, R. Xie, J.H. Jonason, X. Tan, W. Hou, D. Reynolds, W. Hsu, S.E. Harris, J.E. Puzas, H. Awad, R.J. O'Keefe, B.F. Boyce, D. Chen, Axin2 controls bone remodeling through the beta-catenin-BMP signaling pathway in adult mice, *J. Cell Sci.* 122 (Pt 19) (2009) 3566–3578.
- [56] A. Cerqueira, F. Romero-Gavilán, I. García-Arnáez, C. Martínez-Ramos, S. Ozturan, I. Iloro, M. Azkargorta, F. Elortza, R. Izquierdo, M. Gurruchaga, I. Goñi, J. Suay, Bioactive zinc-doped sol-gel coating modulates protein adsorption patterns and in vitro cell responses, *Mater. Sci. Eng. C Mater. Biol. Appl.* 121 (2021) 111839.
- [57] Z. Guo, W. Chen, G. Dai, Y. Huang, Cordycepin suppresses the migration and invasion of human liver cancer cells by downregulating the expression of CXCR4, *Int. J. Mol. Med.* 45 (1) (2020) 141–150.
- [58] L. Tian, K. Wang, H. Liu, K. Li, B. Lin, Z. Fang, J. Han, N. Li, H. Yang, L. Bian, X. Liu, Z. Xi, UCH-L1 mitigates neurotoxicity induced by ZnO particles via stabilizing the inhibitor of NF- κ B signaling, I κ B- α , *Ecotoxicol. Environ. Saf.* 180 (2019) 259–268.
- [59] Y.S. Cho, H.K. Kim, M.S. Ghim, M.W. Hong, Y.Y. Kim, Y.S. Cho, Evaluation of the antibacterial activity and cell response for 3D-printed polycaprolactone/nanohydroxyapatite scaffold with zinc oxide coating, *Polymers* 12 (10) (2020).
- [60] H. Maleki-Ghaleh, M. Hossein Siadati, A. Fallah, A. Zarrabi, F. Afghah, B. Koc, E. Dalir Abdollahinia, Y. Omid, J. Barar, A. Akbari-Fakhrabadi, Y. Beygi-Khosrowshahi, K. Adibkia, Effect of zinc-doped hydroxyapatite/graphene nanocomposite on the physicochemical properties and osteogenesis differentiation of 3D-printed polycaprolactone scaffolds for bone tissue engineering, *Chem. Eng. J.* 426 (2021) 131321.